# Dimeric Rare Earth BINOLate Complexes: Activation of 1,4–Benzoquinone through Lewis-Acid Promoted Potential Shifts

**Jerome R. Robinson,[a] Corwin H. Booth,[b] Patrick J. Carroll,[a] Patrick J. Walsh,[a]* and Eric J. Schelter[a]***

**Abstract:** Reaction of *p*–benzoquinone (BQ) with a series of rare earth/alkali metal/1,1′–BINOLate (REMB) complexes (RE: La, Ce, Pr, Nd; M: Li) results in the largest recorded shift in reduction potential observed for BQ upon complexation. In the case of cerium, the formation of a 2:1 [Ce]:[BQ] complex shifts the two electron reduction of BQ by ≥ 1.6 V to a more favourable potential. Reactivity investigations were extended to other $RE^{III}$ (RE = La, Pr, Nd) where the resulting highly electron deficient quinone ligands afforded isolation of the first lanthanide quinhydrone-type charge transfer complexes. The large reduction potential shift associated with the formation of 2:1 [Ce]:[BQ] complexes illustrate the potential of Ce complexes to function both as a Lewis acids and electron sources in redox chemistry and organic substrate activation.

**Keywords:** lanthanides •oxidation • electrochemistry • magnetism • spectroscopy

## Introduction

Electron transfer (ET) reactions play an important role in chemical and biological systems.[1] In many cases, ET is enabled in Nature or in synthetic systems through the action of Lewis acidic metal cations.[2] Coordination of a Lewis basic electron acceptor to Lewis acidic metal cations can impact both the thermodynamic potential of the electron acceptor and the reorganization energy associated with the ET process.[2e-g] For the purposes of this work, we refer to the positive shift in the thermodynamic reduction potential of the electron acceptor upon coordination to a Lewis acid as Lewis Acid Promoted Potential **S**hift (LAPPS). Trivalent rare earth ($RE^{III}$) cations display the largest recorded LAPPS due the high Lewis acidity associated with these ions.[3] In the most dramatic examples, an ET process that is unfavorable (endergonic) in the absence of a Lewis acid occurs at an appreciable rate in the presence of a Lewis acid.[2f, g] For example, the oxidation of cobalt tetraphenylphorphyrin, $E°_{ox}$ = 0.35 V *vs* SCE in MeCN, with *p*–benzoquinone (BQ), $E°_{red}$ = –0.51 V *vs* SCE in MeCN, is endergonic; however, addition of strong Lewis acids such as $Sc(OTf)_3$ results in a ~1 V shift in the oxidation potential of BQ and a rapid ET event.[3a]

While there are several examples of $RE^{III}$ inducing LAPPS,[2f, g, 3] there has been no investigation of $RE^{III}$ cations acting as both a Lewis acid in the activation of electron acceptors and as the electron donor. Cerium is the only rare earth ion with appreciable chemistry in the +4 oxidation state, which is necessary for the $RE^{III}$ to act as an electron donor.[4] To investigate the impact of LAPPS with $Ce^{III}$ complexes, we were interested in systems where (*1*) the cerium(III) ion is accessible to coordination by the Lewis basic oxidant, and (*2*) the formal potentials of the donor and acceptor alone are endergonic. With this in mind, we chose to investigate the reactivity of the electron-rich heterobimetallic framework $[Li_3(THF)_4][(BINOLate)_3Ce–(THF)]$, **1–Ce**, $E_{pa}$ = –0.45 V *vs* Fc in THF,[5] with the formally weak oxidant, *p*–benzoquinone, BQ, $E_{BQ/BQ^-}$ = –1.03 V and $E_{BQ^-/BQ2^-}$ = –2.05 *vs* Fc in THF. We hypothesized that the sterically accessible cerium(III) center of **1–Ce** could induce activation of BQ, especially through dual coordination of BQ to form a 2:1 Ce:BQ complex.

Herein we report the successful isolation of a rare, stable dimeric $Ce^{IV}$ complex, which displays the largest LAPPS observed for complexation by lanthanide cations (≥ 1.6 V). We also extended our reactivity investigations of BQ to $Pr^{III}$ and $Nd^{III}$ ions in the same

[a] Department of Chemistry, University of Pennsylvania
231 S. 34th St. Philadelphia, PA 19104 (USA)
Fax: (+) (215) 573-2112
Tel: (+) (215) 898-8633, (215) 573-2875
E-mail: pwalsh@sas.upenn.edu, schelter@sas.upenn.edu

[b] 1 Cyclotron Rd. MS70A-1150
Chemical Sciences Division, Lawrence Berkeley National Laboratory
Berkeley, CA 94720, United States
Fax: + (510) 486-5596
Tel (510) 486-6079
E-mail:chbooth@lbl.gov

Supporting information for this article is available on the WWW under http://www.chemeurj.org/ or from the author.

heterobimetallic framework, and isolate the first examples of RE quinhydrone-type intramolecular charge transfer complexes.

## Results and Discussion

### Synthesis and Characterization of Ce–BQ Complex (2–Ce)

We began our investigations with the reaction of **1–Ce** with BQ. Layering of a yellow $Et_2O$ solution BQ upon a pale yellow $Et_2O$ solution of **1–Ce** produced an immediate color change to dark purple (Scheme 1). Layering of pentane on the intense purple solution induced crystallization of $[Li_6(Et_2O)_7][(BINOLate)_6Ce_2(\mu\text{–}O_2C_6H_4)]\cdot Et_2O$ (**2–Ce**) as an analytically pure material in 89 % yield. This reaction is insensitive to the presence of coordinating solvent, such as THF, or to the stoichiometry of BQ. Complex **2–Ce** was the only crystalline product isolated from the reaction. The solution UV-Vis absorption spectrum measured for **2–Ce** in THF showed a broad, intense feature centered at ~480 nm with ε = 13,800 $M^{-1}$ $cm^{-1}$ that was assigned to a LMCT band from the BINOLate ligands to the formal $Ce^{IV}$ ion, similar to that observed for $[Li_3(THF)_4][(BINOLate)_3Ce^{IV}\text{–Cl}]$ at 487 nm.[5] The X-ray crystal structure of **2–Ce** confirmed the 2:1 ratio of cerium to BQ (Figure 1).

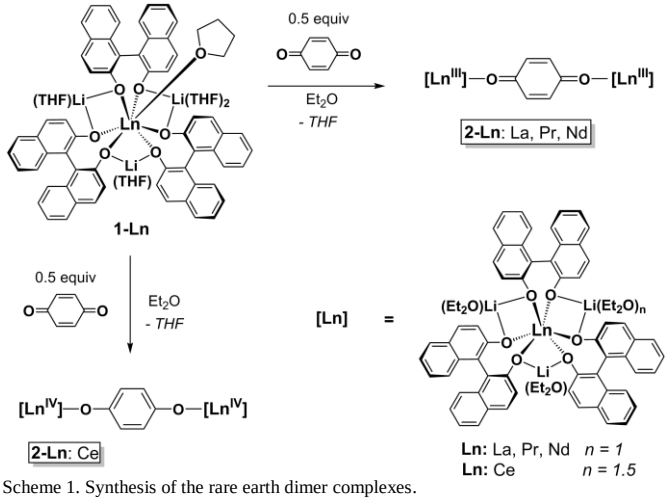


Scheme 1. Synthesis of the rare earth dimer complexes.

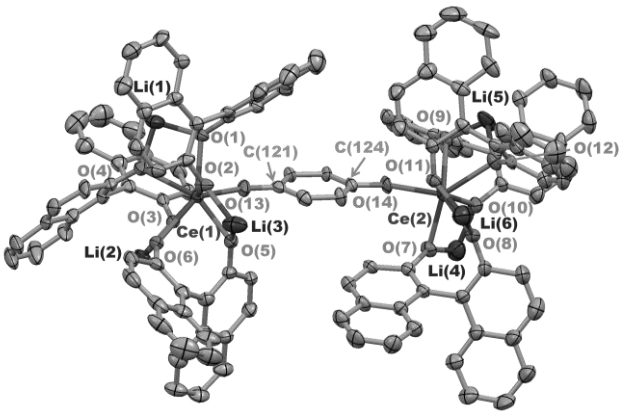


Figure 1. Thermal ellipsoid plot of 2 with 50% probability ellipsoids. Solvent molecules and hydrogen atoms have been removed for clarity.

The C–C, C–O, and O–Ce bond distances for the BQ ligand in **2–Ce** are presented in Table 1 and support the assignment of a fully reduced $BQ^{2-}$ moiety. In all cases the bond distances within the $BQ^{2-}$ ligand are similar to the single structurally characterized Ce-BQ complex, $[[(^tBu_3CO)_3Ce]_2(\mu\text{–}O_2C_6H_4)]$ (**3**).[6] The $Ce\text{–}O_{BQ2-}$ distances in **2–Ce** are 2.124(5) and 2.143(5) Å, which are slightly longer than the 2.086(10) Å $Ce\text{–}OBQ^{2-}$ distance observed in **3**, presumably due to larger steric hindrance between the two halves of the complex in **2–Ce** compared to **3**. It is noteworthy that complex **2–Ce** displays no signs of decomposition in the solid state or in solution, whereas **3** is unstable in the solid state and decomposes to unknown paramagnetic products. We attribute the stability of **2–Ce** to its interlocked heterobimetallic framework. The solution structure of **2–Ce** reflects the dimeric solid state structure; $^1H$ and $^{13}C\{^1H\}$ NMR spectra taken in THF–$d_8$ for **2–Ce** display 21 of the expected 22 $^{13}C\{^1H\}$ aryl resonances for broken $D_3$ solution symmetry (see Supporting Information).

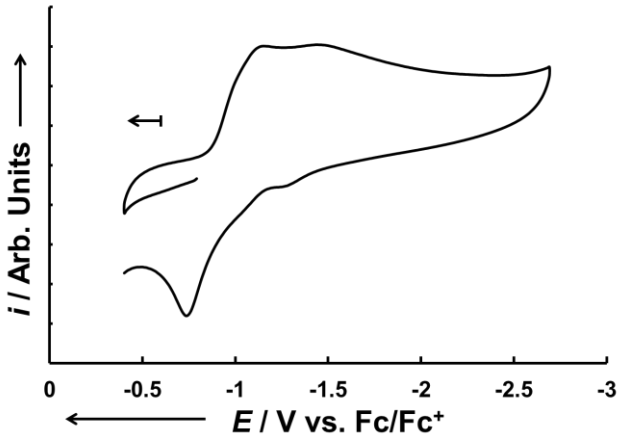


Figure 2. Cyclic voltammogram of the isolated $Ce^{IV/III}$ couple of **2–Ce** in THF (v = 500 mV $s^{-1}$; [**2–Ce**] = 1 mM; $[NPr_4][BArF]$ = 0.1 M)

Ce complexes are known to show valence ambiguity when coordinated by redox active ligands.[7] Further support for the assignment of the canonical $Ce^{IV}$ oxidation state in **2–Ce** was established through solution electrochemical measurements (Figure 2). The measured rest potential in this experiment was –0.80 V versus Fc. Successive quasi-reversible metal reductions for **2–Ce** were observed at $E_{pc}$ = –1.15 V and –1.45 V *vs* Fc and represent a stabilization of the $Ce^{III}/Ce^{IV}$ oxidation wave by ~2.5 V as compared with the standard potential reported for the ion. Electrochemical reversibility was not improved by isolating either of the metal-based reduction waves, and the oxidation waves exhibited complex scan-rate dependent behavior (see Supporting Information). The potentials of these metal reductions are comparable to the voltammogram of **1–Ce** observed in our previous report at $E_{pc}$ = –1.27 V. [5]

Final assignment of the $Ce^{IV}$ state was made through $L_{III}$ edge XANES spectra, which were collected for **1–Ce** and **2–Ce** (Figure 3). As expected, the single edge feature at ~5725 eV for **1–Ce** is consistent with a $Ce^{III}$ complex, whereas the split feature for **2–Ce** centered at ~5730 eV supports bona fide $Ce^{IV}$ ions. No temperature dependence of the XANES was observed between 30 K and 300 K. This data represents the only authenticated $Ce^{IV}\text{–}Ce^{IV}$ quinone dimer by XANES, and confirms the ground state of **2–Ce** as purely $Ce^{IV}\text{–}Ce^{IV}$.

Although BQ has previously been used as an oxidant in cerium chemistry,[6, 7d, e, 8] the oxidation of $Ce^{III}$ complexes with BQ is surprising because BQ is a weak oxidant, and cerium(III) is a weak reductant. However, the observation of a fully reduced BQ moiety, as in **2–Ce**, corresponds to a $\Delta E_{pc}$ of the overall two electron

Table 1. Selected bond distances for the BQ ligand in **2–Ce**, **2–Pr**, and **2–Nd**.

| Bond Distances [Å] | **2–Ce** | | **2–Pr** | | **2–Nd** | |
|---|---|---|---|---|---|---|
| $Ln–O_{BQ}$ | Ce(1)–O(13) | 2.124(5) | Pr(1)–O(13) | 2.636(4) | Nd(1)–O(13) | 2.626(4) |
| | Ce(2)–O(14) | 2.143(5) | Pr(2)–O(14) | 2.624(4) | Nd(2)–O(14) | 2.600(4) |
| $C_{ring}–C_{ring}$ | C(122)–C(123) | 1.401(9) | C(122)–C(123) | 1.320(6) | C(122)–C(123) | 1.325(6) |
| | C(125)–C(126) | 1.388(10) | C(125)–C(126) | 1.340(6) | C(125)–C(126) | 1.346(6) |
| $C_{ring}–C_{ipso}$ | C(121)–C(122) | 1.390(10) | C(121)–C(122) | 1.470(6) | C(121)–C(122) | 1.478(6) |
| | C(121)–C126) | 1.380(10) | C(121)–C126) | 1.474(7) | C(121)–C126) | 1.458(7) |
| | C(123)–C(124) | 1.372(10) | C(123)–C(124) | 1.487(7) | C(123)–C(124) | 1.473(7) |
| | C(124)–C(125) | 1.384(10) | C(124)–C(125) | 1.464(6) | C(124)–C(125) | 1.468(6) |
| $C_{ipso}–O_{BQ}$ | O(13)–C(121) | 1.341(8) | O(13)–C(121) | 1.236(6) | O(13)–C(121) | 1.248(6) |
| | O(14)–C(124) | 1.340(8) | O(14)–C(124) | 1.128(6) | O(14)–C(124) | 1.235(6) |

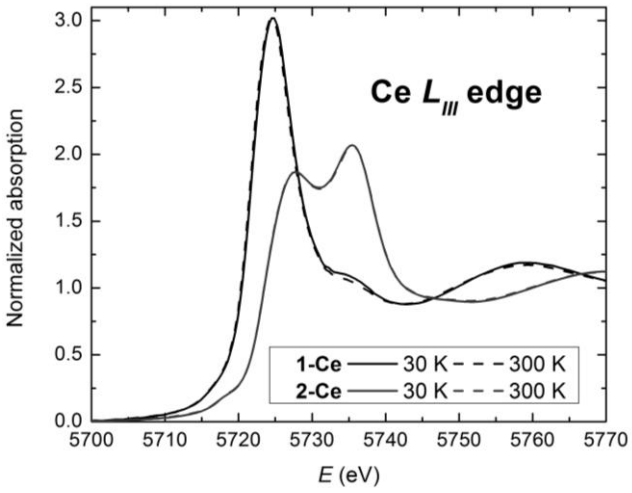


Figure. 3 Ce LIII edge XANES data for **1–Ce** and **2–Ce** at 30 and 300 K.

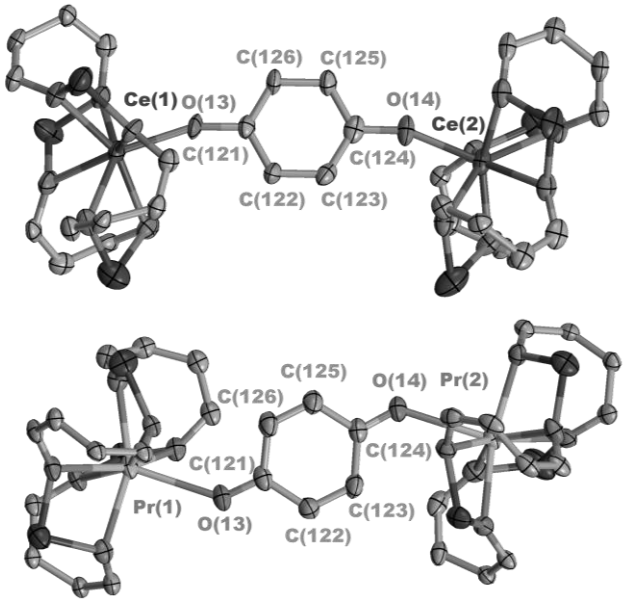


Figure 4. Comparison of the 50 % thermal ellipsoid plots of **2–Ce** (upper) and **2–Pr** (lower). The solvent and most BINOLate carbon atoms are removed.

reduction process for BQ by greater than ~1.6 V, which is the largest LAPPS observed for coordination to a lanthanide.[2f, 9]‡ The considerable LAPPS indicate that 2:1 Ce:BQ complex formation strongly activates the BQ moiety, and increases the likelihood of oxidation of other $RE^{III}$ ions upon BQ coordination.

**Synthesis and Properties of Ln-BQ Complexes (2–Ln, Ln = Pr and Nd)**

Encouraged by the unprecedented LAPPS of the BQ in **2–Ce,** we were interested in extending our investigation to the similarly sized $Pr^{III}$ and $Nd^{III}$ ions within the tris(BINOLate) framework. By way of comparison, the next most oxidatively accessible tetravalent lanthanide ions are Tb $E^\circ$ = +3.1 V, Pr: $E^\circ$ = +3.2 V, Nd: $E^\circ$ = +5.0 V, and Dy $E^\circ$ = +5.2 V *vs* NHE.[10] Although examples of $Ln^{IV}$ = Tb, Pr, Nd and Dy are established in solid state chemistry,[11] their large formal oxidation potentials have prevented isolation of molecular complexes of those ions.[12] We hypothesized that as in the case of **2–Ce**, the highly activated, doubly coordinated BQ ligand could overcome these large formal oxidation potentials and induce changes in valence at Pr and Nd in the tris(BINOLate) framework.

We prepared and crystallized known $[Li_3(THF)_4][(BINOLate)_3Ln(THF)]$ Ln = Pr (**1–Pr**) and Nd (**1–Nd**).[13] The crystal structure of **1–Pr** was reported previously, while the new structure of **1–Nd** is provided as supporting information. Interestingly, reaction of **1–Pr** and **1–Nd** with 0.5 equiv of BQ in $Et_2O$ produced intense blue products (Scheme 1). X-ray structures of the complexes also revealed dimeric complexes, $\{[Li_3(Et_2O)_3][(BINOLate)_3Ln]\}_2(\mu–O_2C_6H_4)\cdot 2Et_2O$ Ln = Pr (**2–Pr**), Nd (**2–Nd**), Figure 4, which are unique examples of BQ complexes of those ions. Unlike **2–Ce**, however, the bond distances displayed in Table 1 indicate the BQ ligands in **2–Pr** and **2–Nd** are most consistent with the neutral, quinoid redox form. In light of the intense blue colors of **2–Pr** and **2–Nd**, magnetic susceptibility studies were conducted to detect changes in the 4f valence of the Pr or Nd ions upon coordination of BQ.

The temperature dependent χT product for the complexes **2–Pr** and **2–Nd** were measured between 2–300 K and field dependent measurements were performed at 2 K. The data for **1–Pr** and **2–Pr** are shown in Figure 5, while data for **1–Nd** and **2–Nd** are provided as supporting information. The temperature dependent χT products

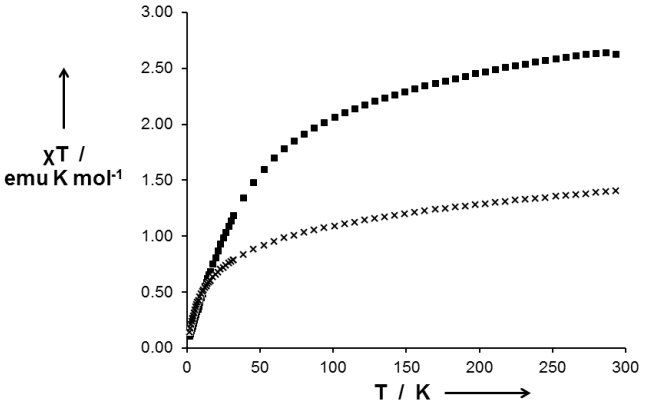


Figure 5. Temperature dependent magnetic data for **1–Pr** (■) and **2–Pr** (X).

for monomeric **1–Pr** and dimeric **2–Pr** were 1.40 and 2.63 emu K mol$^{-1}$, respectively, at 300 K. The value for **1–Pr** of half the value of **2–Pr** at 300 K are both consistent with room temperature χT products for reported $Pr^{III}$ complexes,[4a, 14] which are typically lower than the predicted value from *L–S* coupling of 1.60 emu K mol$^{-1}$. **1–Pr** and **2–Pr** exhibited similar temperature dependences of the χT products, both decrease monotonically primarily due to the depopulation of Stark sublevels with decreasing temperature. Both **1–Pr** and **2–Pr** attain small values at 2 K, 0.14 and 0.10 emu K mol$^{-1}$ respectively, which are consistent with orbital singlet ground states arising from a $4f^2$ electronic configuration and the presence of trace, extrinsic paramagnetic impurities in both cases. The field dependent data for the complexes do not saturate but attain small values of 0.58 and 0.54 $\mu_B$ for the monomer and dimer respectively.

The magnetic data for the dimeric complex **2–Pr** definitively establishes $Pr^{III}$ ions whose valences are unperturbed by the coordinated BQ ligand. As in **1–Pr** and **2–Pr**, the Nd monomer/dimer **1–Nd** and **2–Nd** are consistent with canonical trivalent metal oxidation states. These data are further supported by solution electrochemical measurements, (see Supporting Information), which display redox features for neutral BQ and ligand oxidation features of the tris(BINOLate) framework. Despite the assignment of **2–Pr** and **2–Nd** as trivalent, we were compelled to determine the origin of the intense blue color, and therefore set out to investigate their electronic structures.

### Solution Behavior and Electronic Structure of Ln-BQ Complexes: 2–Ln; Ln = La, Pr, and Nd

To provide insight into the nature of the neutral coordinated BQ electronic structures, we synthesized similarly intense blue **2–La**. Unlike **2–Ce**, we noted that the dissolution of **2–La**, **2–Pr**, or **2–Nd** at low concentrations in THF–$d_8$ resulted in loss of the intense colors observed in the solid state. We hypothesized the bleaching of the dark colors for **2–Ln** (Ln = La, Pr, Nd) was due to dissociation of the BQ ligand in those complexes to **1–Ln** and free BQ. Comparison of the $^1$H-NMR spectra of the diamagnetic complexes **2–Ce** and **2–La** suggests differences in substitutional lability of BQ between the complexes (Figure 6). Both $^1$H and $^{13}$C{$^1$H}-NMR of **2–Ln** (Ln = La, Pr, Nd) display $D_3$ symmetry, which is identical to **1–Ln** except for the additional peaks corresponding to free BQ. In contrast, **2–Ce** maintains the expected $C_3$ symmetry in THF–$d_8$ solution, as indicated in the $^1$H and $^{13}$C{$^1$H}-NMR spectra, corresponding to the solid state structure of the complex.

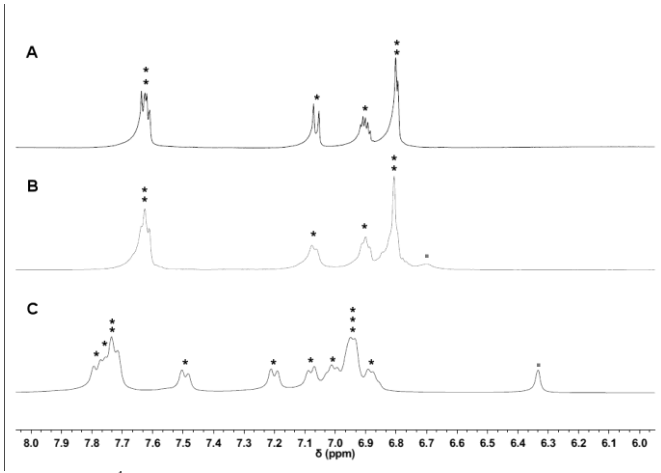


Figure 6. $^1$H-NMR of **1–La** (A), **2–La** (B), and **2–Ce** (C). * = BINOLate resonances; ■ = BQ resonances

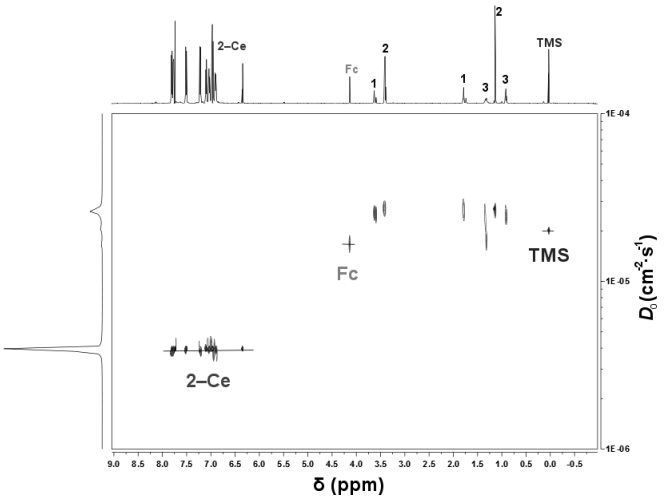


**Figure 7**. $^1$H DOSY NMR spectrum of **2–Ce** and internal references at 300K in THF-$d_8$. Additional peaks (1–3) correspond to solvent impurities: 1 = THF, 2 = $Et_2O$, 3 = Pentane.

Table 2. $D_o$ and $r_H$ for internal standards and **1–La**, **2–La**, and **2–Ce**

| Compound | $D_o$ ($\times 10^{-6}$ cm$^2$ s$^{-1}$) | $r_{H(exp)}$ (Å)[a] | $r_{H(exp)}$ (Å)[b] | $r_{H(avg)}$ (Å)[c] | $r_{H(theo)}$ (Å)[d] |
|---|---|---|---|---|---|
| **TMS** | 21.2 (4)[e] | – | – | – | 2.365 (6) |
| **Fc** | 16.5 (5) | – | – | – | 2.790 (2) |
| **1–La** | 5.55 (3) | 9.24 (3) | 8.60 (3) | 8.92 (45) | 8.854 (2) |
| **2–La** | 5.15 (5) | 9.63 (3) | 8.76 (3) | 9.20 (61) | 8.854 (2) |
| **2–Ce** | 3.94 (2) | 12.6 (3) | 11.5 (3) | 12.0 (73) | 12.548 (2) |

[a] – Based on $r_{H(theo)}$ for TMS. [b] – Based on $r_{H(theo)}$ for Fc. [c] – Average of $r_{H(theo)}$ for both TMS and Fc. [d] – $r_{H(theo)}$ determined from crystal structures; see Supporting Information for further experimental details. [e] – Standard deviation in parenthesis.

To further support our hypothesis for the dissociation of **2–Ln** (Ln: La, Pr, Nd) in THF, **D**iffusion **O**rdered $^1$H-NMR **S**pectroscop**Y** (DOSY) was performed on the diamagnetic compounds of interest. DOSY experiments for **1–La**, **2–La**, and **2–Ce** were performed in THF–$d_8$ at 300 K in the presence of two internal references, tetramethylsilane (TMS) and ferrocene (Fc). Measured diffusion coefficients ($D_o$) and calculated hydrodynamic radii ($r_H$) are displayed in Table 2, and a representative DOSY spectrum for **2–Ce** is displayed in Figure 7. The data indicate that **1–La** and **2–La** diffuse at similar rates, and their calculated $r_H$ values, $r_{H(exp)}$, agree well with theoretical $r_H$ values, $r_{H(theo)}$ for monomeric solution structures. In contrast, **2–Ce** diffuses at a significantly slower rate, where $r_{H(exp)}$ is consistent with a dimeric solution structure (see Supporting Information for details). These results clarify the solution behavior of **2–Ln** (Ln = La, Pr, Nd). In THF solutions, BQ dissociates from **2–Ln**, because at high THF concentration, the equilibrium favours the dissociation of BQ. For **2–Ce** the binding affinity is much higher for the anionic $BQ^{2-}$ ligand, preserving the dimeric structure of **2–Ce** in THF solution.

The dissociation of **2–Ln** (Ln = La, Pr, Nd) in THF was also evident in the electrochemical data for the complexes. Cyclic voltammograms of **2–Ln** were consistent with both free **1–Ln** and free BQ in THF solutions (Figure 8 and Supporting Information). Reduction potentials observed at ~$E_{1/2}$ = –1.03 V upon dissolution of **2–Ln** (Ln = La, Pr, Nd) were similar for all three complexes and were consistent with the first single-electron reduction observed for free BQ. This is surprising given the large LAPPS observed with **1–Ce** to obtain tetravalent **2–Ce**; however, the negligible shifts in the formal potential of BQ can be rationalized by the small percentage

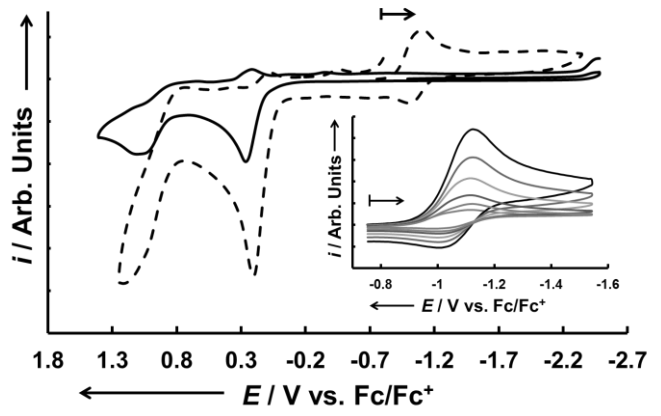


Figure 8. Cyclic voltammograms for **1–Nd** (–) and **2–Nd** (– –) in THF (ν = 500 mV $s^{-1}$; [**1–Nd**] = 0.1 M; [**2–Nd**] = 1 mM; $[NPr_4][BAr^F{}_4]$ = 0.1 M). Inset displays scan rate dependence of the isolated BQ reduction for **2–Nd**.

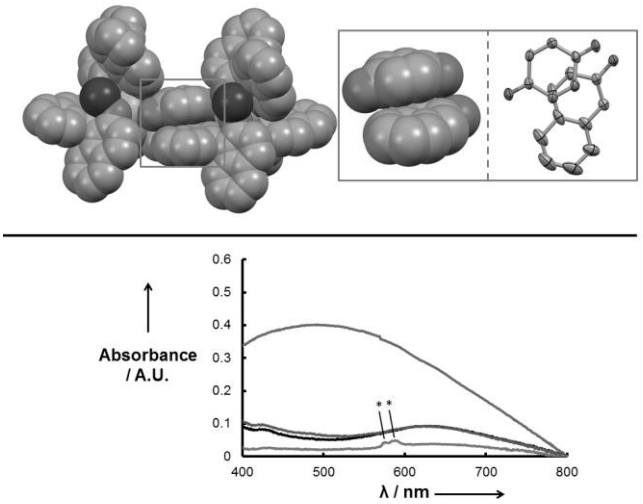


Figure 9. Solid state structure of **2–Pr** (solvent molecules removed for clarity) illustrating the 'short-circuiting' CT interaction in the solid state (top). UV-Visible diffuse reflectance spectra for **2–Ce** (purple), **2–La** (black), **2–Pr** (green), and **2–Nd** (blue), with f – f transitions for **2–Nd** marked with asterisks (*, bottom).

of **1–Ln** coordinated to BQ in solution. It is important to note that the low binding affinity of **1–Ln** for BQ in THF solutions does not prevent activation of BQ, **1–Ce** rapidly reacts with BQ in THF solution to yield **2–Ce**.

We observed no metal-based oxidations in the electrochemical traces of **1–Ln** or **2–Ln** (Ln = La, Pr, Nd), however, we did observe very similar irreversible oxidations events centered around ~0.25 V and 1.0 V *vs* Fc between the complexes. We have assigned these oxidations as BINOLate-based, given their similar oxidation potentials throughout the series (Figure 8 and Supporting Information). Further investigation of the solution properties of **2–Ln** in weakly coordinating and non-coordinating solvents were prevented by their insolubility in these solvents including diethyl ether, toluene, fluorobenzene, and dichloromethane.

**Solid State Characterization of Properties of Ln-BQ Complexes: 2–Ln; Ln = La, Pr, and Nd**

Given the lability of the BQ moiety in coordinating solvents for **2–Ln** (Ln = La, Pr, Nd), we collected electronic absorption spectra on solid samples using diffuse reflectance measurements to investigate the electronic structures of the **2–Ln** complexes. The diffuse reflectance data for the **2–Ln** complexes reveal a broad feature centered at ~625 nm (Figure 9) that is also observed with near saturated solutions, ~50 mM in THF (see Supporting Information). This feature is distinctly different than that of the LMCT band observed for $Ce^{IV}$ in **2–Ce**, which is much more intense in both solution and the solid state and centered at ~480 nm. The physicochemical origin of the broad feature in **2–La**, **2–Pr**, and **2–Nd** is made clear upon examination of their solid state structures; the neutral bridging BQ is within the van der Waals radii of one naphtholate fragments from a coordinated BINOLate ligand (Figure 9), forming an intramolecular charge-transfer (CT) complex.

Charge transfer complexes between arene donors and quinoid acceptors, such as quinhydrones, are well documented for the main-group and transition metals,[15] however, **2–La**, **2–Pr**, and **2–Nd** are the first examples of Ln complexes exhibiting this phenomena. We attribute the intense colors of **2–La**, **2–Pr**, and **2–Nd** to intramolecular CT interactions rather than charge transfer bands involving a change in metal valence. Typically, quinhydrone or phenol-quinone CT complexes involve non-covalent interactions such as hydrogen bonding and π-π stacking to assemble CT interactions, and the CT $\lambda_{max}$ are very sensitive to arenes substitution pattern and solvents.[15d, e] In contrast, the solution CT interactions observed for **2–Ln** are weak, concentration dependent in THF and present primarily in the solid state. The activated quinone is stabilized through the intramolecular donor-acceptor (D–A) interaction formed by the ligand framework; the reduced BINOLate fragment transfers electron density into the electron deficient BQ system. However, the overall contribution of this interaction is weak; the D–A formation seemingly has minimal impact on the LAPPS observed for coordination of BQ with **1–Ce**, and is only isolable when the ET process is unfavourable, when Ln = La, Pr, or Nd.

## Conclusion

Using a heterobimetallic lanthanide framework, we have found that a 2:1 [Ce]:BQ complex results in > +1.6 V LAPPS, which is the largest potential shift that has been observed for coordination of an electron acceptor to a lanthanide cation. We attribute the unprecedented activation of BQ to coordination by two Lewis acids. This is the first example where $Ce^{III}$ ions have been shown to shift the formal potential of an electron acceptor to induce oxidation to $Ce^{IV}$. This concept of activating organic substrates with $Ce^{III}$ as a reductant are of general interest; $Ce^{III}$ is the most abundant RE, and with further development could serve as an economical complement to the well-established $Sm^{II}$ based reductants.[16]

Furthermore, the large LAPPS observed when RE = Ce, prompted our investigation of RE = La, Pr, and Nd. In the case of cerium, dimeric $Ce^{IV}$–BQ complexes are the stable products of coordination and oxidation by BQ, and are an authenticated $Ce^{IV}$–$Ce^{IV}$ dimer. In contrast, La, Pr, and Nd coordination of BQ results in the isolation of the first lanthanide compounds featuring intramolecular CT complexes with an electron-deficient quinoid. Further investigation of LAPPS with the intent of oxidizing trans-cerium RE's using electron rich substituted tris(BINOLate) frameworks and more electron-deficient *p*–benzoquinones is currently underway.

## Experimental Section

**Materials and general methods.** All reactions and manipulations were performed under an inert atmosphere ($N_2$) using standard Schlenk techniques or in a Vacuum Atmospheres, Inc. Nexus II drybox equipped with a molecular sieves 13X / Q5 Cu–0226S catalyst purifier system. Glassware was oven-dried overnight at 150 °C prior to use. $^1$H- $^{13}$C{$^1$H}NMR spectra were obtained on a Bruker Uni–400 or on a Bruker AM–500 Fourier transform NMR spectrometer at 400 and 101 MHz or 500 and 126 MHz, respectively. $^7$Li{$^1$H}-NMR were recorded on a Bruker AM-500 Fourier transform NMR spectrometer at 155 MHz. Chemical shifts were recorded in units of parts per million downfield from residual proteo solvent peaks ($^1$H-) or characteristic solvent peaks ($^{13}$C{$^1$H}). The $^7$Li{$^1$H} spectra were referenced to external solution standards of LiCl in $H_2O$ (at zero ppm). All coupling constants are reported in hertz. The infrared spectra were obtained from 400–4000 cm$^{-1}$ using a Perkin Elmer 1600 series infrared spectrometer. The solution UV-Visible absorption spectra were obtained from 1000–225 nm using a Perkin Elmer 950 UV-Vis/NIR Spectrophotometer, and all samples were prepared under an $N_2$ environment. 1 mm pathlength screw cap quartz cells were used with a blank measured before each run. Diffuse reflectance spectra were collected on a Cary 5000 Spectrophotometer using a prepared KBr mull of **2–Ln** (Ln = La, Ce, Pr, Nd; 10.5 mg **2–Ln** : 200 mg KBr). Elemental analyses were performed at the University of California, Berkeley Microanalytical Facility using a Perkin-Elmer Series II 2400 CHNS analyzer.

Tetrahydrofuran, diethyl ether, dichloromethane, hexanes, and pentane were purchased from Fisher Scientific. The solvents were sparged for 20 min with dry $N_2$ and dried using a commercial two-column solvent purification system comprising columns packed with Q5 reactant and neutral alumina respectively (for hexanes and pentane), or two columns of neutral alumina (for THF, $Et_2O$ and $CH_2Cl_2$). Deuterated solvents were purchased from Cambridge Isotope Laboratories, Inc. and stored over potassium mirror overnight prior to use. Cerium(III) triflate (Strem Chemicals Inc.) was heated at 150 °C for 12 hours at ~100 mtorr prior to use. 1,4-Benzoquinone was purchased from Acros Organics and sublimed before use. Trityl chloride was purchased from Acros Organics and used without further purification. $Ce(N(TMS)_2)_3$,[17] $Li_2$(*S*-BINOLate), $[Li_3(THF)_4][(BINOLate)_3Ln(THF)]\cdot THF$ (Ln = La, Ce, Pr)[5a, 13] and the supporting electrolyte, $[^nPr_4N][B(3,5\text{-}(CF_3)_2\text{-}C_6H_3)_4]$,[18] were prepared according to literature procedures.

**Synthesis of $[Li_3(THF)_4][(BINOLate)_3Nd(THF)]\cdot THF$ (1–Nd).** A 20 mL scintillation vial was charged with $Nd(OTf)_3$ (1.00 g, 1.69 mmol; FW: 591.45), (*S*)–BINOL (1.45 g, 5.07 mmol, 3 equiv; FW: 286.32), THF (15 mL), and a Teflon-coated stir bar. $LiN(SiMe_3)_2$ (1.70 g, 10.1 mmol, 6 equiv; FW: 167.32) was added as a solid with an immediate color change to light blue. After 5 min the solution became clear, and the solution was stirred at room temperature for an additional 2 h. Solvents were removed under reduced pressure, extracted with toluene (20 mL), and filtered through a Celite-padded coarse porosity fritted filter. The solvent was removed under reduced pressure and the light blue powder was redissolved in minimal THF (10 mL) and layered with hexane in 1:4 volumetric ratio. Light blue crystals of **1–Nd** were isolated by vacuum filtration over a medium porosity fritted filter, washed with hexane (3 × 5 mL), and dried for 3 h under reduced pressure. Light blue X-ray quality crystals were obtained by vapor diffusion of pentane into a concentrated THF solution of **1–Nd**. Yield 1.83 g (1.26 mmol, 75% yield; FW: 1450.58). Anal. Calcd for $C_{84}H_{84}O_{12}Li_3Nd$: C, 69.55; H, 5.84. Found: C, 69.23; H, 5.48. $^1$H NMR (500 MHz, THF–$d_8$) δ: 11.53 (d, $J$ = 8.3 Hz, 2H), 8.83 (t, $J$ = 7.7 Hz, 2H), 7.71 (dd, $J$ = 14.9, 7.5 Hz, 4H), 5.25 (s, 2H), -4.98 (s, 2H); $^7$Li{$^1$H} NMR (155 MHz, THF–$d_8$) δ: 27.7 (s); $^{13}$C{$^1$H} NMR (126 MHz, THF–$d_8$) δ: 161.4, 139.1, 139.0, 133.1, 133.1, 129.4, 128.1, 126.4, 124.7, 123.8. IR (KBr, cm$^{-1}$) *v*: 3048, 2977, 2878, 1614, 1590, 1556, 1501, 1464, 1423, 1362, 1352, 1341, 1273, 1248, 1211, 1180, 1143, 1126, 1070, 1046, 995, 957, 936, 894, 859, 821, 790, 775, 821, 746, 692, 634, 665, 576, 487 cm$^{-1}$.

**Synthesis of $[[Li_3(Et_2O)_4][(BINOLate)_3Ce]_2(\mu\text{–}O_2C_6H_4)$ (2–Ce).** A 20 mL vial was charged with $[Li_3(THF)_4][(BINOLate)_3Ce(THF)]\cdot THF$ (150 mg, 0.104 mmol; FW: 1446.5 ) and $Et_2O$ (3 mL). 1,4–benzoquinone (5.6 mg, 0.052 mmol, 0.5 equiv; FW: 108.10) was layered as an $Et_2O$ solution (1 mL), and there was an immediate color change at the interface to dark purple. Additional $Et_2O$ (~1 mL) was layered, followed by pentane (12 mL). The reaction was left overnight to yield dark purple crystals. The crystals were isolated by vacuum filtration over a medium porosity fritted filter, washed with hexanes (5 mL), and dried for 3 h under reduced pressure. X-ray quality single crystals were obtained from saturated $Et_2O$ solutions layered with pentane (1:4 volumetric ratio). Yield 126 mg (0.046 mmol, 89% yield; FW: 2728.79). Anal. Calcd for $C_{158}H_{156}O_{22}Li_6Ce_2$: C, 69.54; H, 5.76. Found: C, 69.19; H, 5.46. $^1$H NMR (400 MHz, THF) δ 7.78 (d, $J$ = 8.9 Hz, 6H), 7.74 (t, $J$ = 8.9 Hz, 18H), 7.49 (d, $J$ = 8.9 Hz, 6H), 7.20 (d, $J$ = 8.7 Hz, 6H), 7.08 (d, $J$ = 8.6 Hz, 6H), 7.01 (t, $J$ = 7.6 Hz, 6H), 6.95 (m, 18H), 6.92–6.81 (m, 6H) 6.34 (s, 4H, C–H, hydroquinone). $^7$Li{$^1$H} NMR (155 MHz, THF–$d_8$) δ: –1.71 (s); $^{13}$C{$^1$H} NMR (101 MHz, THF–$d_8$) δ 169.2 (C–O, hydroquinone), 165.3, 164.6, 135.9, 135.5, 129.8, 129.7, 128.6, 128.3, 127.8, 127.7, 127.4, 127.3, 126.3, 125.1, 124.7, 121.7, 121.4, 119.8, 119.0, 118.1. Due to accidental equivalence, 21 of expected 22 resonances were observed. IR (KBr, cm$^{-1}$) ν: 3051, 2978, 2873, 1655 (w), 1614, 1589, 1557, 1501, 14611, 1425, 1362, 1352, 1334, 1274, 1240, 1144, 1127, 1071, 992, 953, 862, 821, 746, 666, 573, 475 cm$^{-1}$.

**Alternate Synthesis of 2–Ce**. A 125 mL side-arm flask was charged with $[Li_3(THF)_4][(BINOLate)_3Ce(THF)]\cdot THF$ (500 mg, 0.346 mmol; FW: 1446.5 ), $Et_2O$ (20 mL), and a Teflon coated stir bar. 1,4–Benzoquinone (18.7 mg, 0.173 mmol, 0.5 equiv; FW: 108.10) was added to the light yellow solution as a solid, followed by an immediate color change to dark purple. The reaction was allowed to stir for an additional two hours, and the solvent volume was reduced to 5 mL under reduced pressure. Hexanes (15 mL) was added and the purple solid was isolated by vacuum filtration over a medium frit and dried for 3 h. Yield 420 mg. (0.154 mmol, 89%).

**General Procedure A: $\{[Li_3(Et_2O)_3][(BINOLate)_3Ln]\}_2(\mu\text{–}O_2C_6H_4)\cdot 2Et_2O$ (2–Ln, Ln = La, Pr, or Nd).** A 20 mL vial was charged with $[Li_3(THF)_4][(BINOLate)_3Ln(THF)]\cdot THF$ (250 mg) and $Et_2O$ (3 mL). 1,4–Benzoquinone (0.5 equiv) was layered as an $Et_2O$ solution (1 mL), and there was an immediate color change at the interface to dark blue/green. Additional $Et_2O$ (~1 mL) was layered, followed by pentane (12 mL). The reaction was set undisturbed for 14 to yield dark blue/green crystals and a blue filtrate. The crystals were isolated by vacuum filtration over a medium porosity fritted filter, washed with minimal amounts of cold $Et_2O$ (3 mL) and hexanes (5 mL), and dried for 3 h under reduced pressure. X-ray quality single crystals were also obtained under these layering conditions.

**$\{[Li_3(Et_2O)_3][(BINOLate)_3La]\}_2(\mu\text{–}O_2C_6H_4)\cdot 2Et_2O$ (2–La).** Prepared following general procedure A. 199 mg (0.0728 mmol, 84% yield; FW: 2726.37) Anal. Calcd for $C_{158}H_{156}O_{22}Li_6La_2$: C, 69.60; H, 5.77. Found: C, 69.28; H, 5.61. $^1$H NMR (500 MHz, THF–$d_8$) δ: 7.66 (t, $J$ = 7.5 Hz, 24H), 7.10 (d, $J$ = 8.8 Hz, 12H), 6.94 (t, $J$ = 6.9 Hz, 12H), 6.84 (s, 24H), 6.74 (s, 4H, C–H, Quinone); $^7$Li{$^1$H} NMR (155 MHz, THF–$d_8$) δ: 3.4 (s); $^{13}$C{$^1$H} NMR (126 MHz, THF–$d_8$) δ187.9 (C=O, Quinone), 163.3, 137.2 (C–H, Quinone), 136.6, 128.3, 128.3, 128.0, 126.8, 124.7, 120.3, 119.0 IR (KBr, cm$^{-1}$) *v*: 3048, 2975, 2876, 1655 (C=O, quinone, s), 1614, 1590, 1556, 1500, 1463, 1423, 1362, 1352, 1341, 1273, 1247, 1211, 1143, 1126, 1071, 1046, 993, 957, 935, 881, 859, 821, 745, 691, 664, 633, 575, 487 cm$^{-1}$.

**$\{[Li_3(Et_2O)_3][(BINOLate)_3Pr]\}_2(\mu\text{–}O_2C_6H_4)\cdot 2Et_2O$ (2–Pr).** Prepared following general procedure A. 180 mg (0.0658 mmol,

76% yield; FW: 2730.39) Anal. Calcd for $C_{158}H_{156}O_{22}Li_6Pr_2$: C, 69.50; H, 5.76. Found: C, 69.82; H, 5.83. $^1$H NMR (500 MHz, THF–$d_8$) δ: 14.32 (s, 12H), 9.91 (s, 12H), 8.28 (s, 12H), 7.69 (s, 12H), 6.31 (s, 4H, C–H, Quinone), 3.51 (s, 12H), –11.92 (s, 12H). Note: One of the Ar-H of the BINOLate resonances lies beneath that of the $Et_2O$ solvent peak. This is in agreement with the integration of the $Et_2O$ solvent peaks (see spectrum below). $^7$Li{$^1$H} NMR (155 MHz, THF–$d_8$) δ: 41.2 (s); $^{13}$C{$^1$H} NMR (126 MHz, THF–$d_8$) δ: 176.2, 147.4, 143.7, 136.1 (C-H, Quinone), 135.1, 133.2, 129.0, 127.9, 125.7, 124.1, 123.8. The C=O (quinone) $^{13}$C resonance was not observed and is attributed to the paramagnetism of **2–Pr**. IR (KBr, cm$^{-1}$) *ν*: 3049 2975, 2876, 1655 (C=O, quinone, s), 1614, 1590, 1556, 1501, 1464, 1424, 1362, 1352, 1341, 1274, 11247, 1211, 1144, 1127, 1071, 1046, 993, 957, 935, 881, 860, 822, 746, 692, 665, 633, 576, 484 cm$^{-1}$.

**{[Li$_3$(Et$_2$O)$_3$][(BINOLate)$_3$Nd]}$_2$(μ–O$_2$C$_6$H$_4$)·2Et$_2$O (2–Nd)**. Prepared following general procedure A. 187 mg (0.0684 mmol, 79% yield; FW: 2737.05) Anal. Calcd for $C_{158}H_{156}O_{22}Li_6Nd_2$: C, 69.33; H, 5.74. Found: C, 69.23; H, 5.49. $^1$H NMR (500 MHz, THF–$d_8$) δ: $^1$H NMR (500 MHz, THF-d8) δ 11.58 (d, *J* = 9.0 Hz, 12H), 8.86 (d, *J* = 7.8 Hz, 12H), 8.04 – 7.48 (m, 24H), 6.21 (s, 4H, C–H, Quinone), 5.27 (s, 12H), -5.03 (s, 12H); $^7$Li{$^1$H} NMR (155 MHz, THF–$d_8$) δ: 27.7 (s); $^{13}$C{$^1$H} NMR (126 MHz, THF–$d_8$) δ: 161.4, 139.2, 136.3 (C-H, Quinone), 133.2, 133.1, 129.3, 128.2, 126.4, 124.7, 123.8. Due to overlap (accidental equivalence), 9 of the 10 BINOLate $^{13}$C were observed. Additionally, the C=O (quinone) $^{13}$C resonance was not observed and is attributed to the paramagnetism of **2–Nd**. IR (KBr, cm$^{-1}$) *ν*: 3048, 2971, 2876, 1656 (C=O, quinone, s), 1614, 1590, 1556, 1501, 1463, 1424, 1362, 1352, 1341, 1273, 1248, 1211, 1181, 1143, 1126, 1071, 1045, 994, 957, 936, 881, 860, 821, 745, 691, 665, 634, 576, 487 cm$^{-1}$

**X-ray crystallography.** X-ray intensity data were collected on a Bruker APEXII CCD area detector employing graphite-monochromated Mo-Kα radiation (λ=0.71073 Å) at a temperature of 143(1)K. The crystal of [Li$_3$(THF)$_4$][(BINOLate)$_3$Nd(THF)]·THF (**1**) grew as a non-merohedral twin; the program CELL_NOW[19] was used to index the diffraction images and to determine the twinning mechanism. The crystal was twinned by a rotation of 180° about the c direct axis. In all cases, rotation frames were integrated using SAINT,[20] producing a listing of unaveraged F$^2$ and σ(F$^2$) values which were then passed to the SHELXTL[21] program package for further processing and structure solution on a Dell Pentium 4 computer. The intensity data were corrected for Lorentz and polarization effects and for absorption using TWINABS[22] or SADABS.[23] The structures were solved by direct methods (SHELXS-97).[24] Refinement was by full-matrix least squares based on F$^2$ using SHELXL-97.[24] All reflections were used during refinements. Non-hydrogen atoms were refined anisotropically and hydrogen atoms were refined using a riding model. For the structure **1–Nd** and **2–Pr** there was an area of disordered solvent for which a reliable disorder model could not be devised; the X-ray data were corrected for the presence of disordered solvent using SQUEEZE.[25]

**Crystal data for 1–Nd.** $C_{84}H_{84}O_{12}NdLi_3$. $M_r$ = 1450.57; monoclinic, space group $P2_1$, *a* = 18.2775(12), *b* = 11.4640(7), *c* = 19.0161(12) Å, *α* = 90, *β* = 100.685(3), *γ* = 90°. *V* = 3915.4(4) Å$^3$. *Z*=2, $\rho_{calcd}$=1.230 g cm$^{-3}$, $\mu(Mo_{K\alpha})$=0.721 cm$^{-1}$, $F_{000}$=1506, 2*θ* range=1.71–27.54°, crystal size=0.38 × 0.22 × 0.12 mm$^3$ *T*=143 K; 17685 reflections measured with 16883 used in refinement; $R_1$=0.0233, $wR_2$=0.0671 (16883 reflections with $F>4\sigma(F)$); $R_1$=0.0254, $wR_2$=0.0700, GoF=0.777 (17685 unique, nonzero reflections and 947 variables).

**Crystal data for 2–Ce.** $C_{158}H_{156}O_{22}Ce_2Li_6$. $M_r$ = 2728.71; monoclinic, space group $P2_1$, *a* = 13.8652(18), *b* = 36.747(4), *c* = 14.9515(19) Å, *α* = 90, *β* = 115.301(7), *γ* = 90°. *V* = 6887.1(15) Å$^3$. *Z*=2, $\rho_{calcd}$=1.316 g cm$^{-3}$, $\mu(Mo_{K\alpha})$=0.721 cm$^{-1}$, $F_{000}$=2828, 2*θ* range=1.51–27.72°, crystal size=0.35 × 0.10 × 0.03 mm$^3$ *T*=143 K; 29333 reflections measured with 20416 used in refinement; $R_1$=0.0614, $wR_2$=0.1317 (20416 reflections with $F>4\sigma(F)$); $R_1$=0.1141, $wR_2$=0.1523, GoF=1.021 (29333 unique, nonzero reflections and 1712 variables).

**Crystal data for 2–La.** $C_{166}H_{176}O_{24}La_2Li_6$. $M_r$ = 2874.53; triclinic, space group *P*1, *a* = 15.0573(12), *b* = 15.1269(12), *c* = 19.3604(15) Å, *α* = 90.362(4), *β* = 100.937(4), *γ* = 119.685(3)°. *V* = 3735.3(5) Å$^3$. *Z*=1, $\rho_{calcd}$=1.278 g cm$^{-3}$, $\mu(Mo_{K\alpha})$=0.632 cm$^{-1}$, $F_{000}$=1496, 2*θ* range=1.57–27.50°, crystal size=0.50 × 0.30 × 0.20 mm$^3$ *T*=143 K; 32945 reflections measured with 31522 used in refinement; $R_1$=0.0296, $wR_2$=0.779 (31522 reflections with $F>4\sigma(F)$); $R_1$=0.0318, $wR_2$=0.797, GoF=1.071 (32945 unique, nonzero reflections and 1784 variables).

**Crystal data for 2–Pr.** $C_{166}H_{176}O_{24}Pr_2Li_6$. $M_r$ = 2878.53; triclinic, space group *P*1, *a* = 15.0366(10), *b* = 15.0710(10), *c* = 19.333(2) Å, *α* = 90.341(4), *β* = 101.109(4), *γ* = 119.615(3)°. *V* = 3711.2(5) Å$^3$. *Z*=1, $\rho_{calcd}$=1.288 g cm$^{-3}$, $\mu(Mo_{K\alpha})$=0.717 cm$^{-1}$, $F_{000}$=1500, 2*θ* range=1.79–27.62°, crystal size=0.32 × 0.25 × 0.12 mm$^3$ *T*=143 K; 32634 reflections measured with 29136 used in refinement; $R_1$=0.0412, $wR_2$=0.1059 (29136 reflections with $F>4\sigma(F)$); $R_1$=0.0498, $wR_2$=0.1113, GoF=1.049 (32634 unique, nonzero reflections and 1748 variables).

**Crystal data for 2–Nd.** $C_{166}H_{176}O_{24}Nd_2Li_6$. $M_r$ = 2885.19; triclinic, space group *P*1, *a* = 15.0573(6), *b* = 15.1269(6), *c* = 19.3604(7) Å, *α* = 90.362(1), *β* = 100.937(2), *γ* = 119.685(2)°. *V* = 3735.3(2) Å$^3$. *Z*=1, $\rho_{calcd}$=1.283 g cm$^{-3}$, $\mu(Mo_{K\alpha})$=0.755 cm$^{-1}$, $F_{000}$=1502, 2*θ* range=1.57–27.77°, crystal size=0.32 × 0.24 × 0.12 mm$^3$ *T*=143 K; 33507 reflections measured with 30176 used in refinement; $R_1$=0.0420, $wR_2$=0.1060 (30176 reflections with $F>4\sigma(F)$); $R_1$=0.0498, $wR_2$=0.1122, GoF=1.077 (33507 unique, nonzero reflections and 1784 variables).

Further experimental details are provided as Supporting Information.

## Acknowledgements

E.J.S. and P.J.W. acknowledge the University of Pennsylvania and the NSF (CHE–1026553 and CHE–0840438 for an X-ray diffractometer). We thank Prof. Jay Kikkawa (UPenn) for assistance with the magnetic measurements. The Penn University Research Foundation is acknowledged for support of the Perkin Elmer 950 UV-Vis/NIR Spectrophotometer. We thank the Kagan group (UPenn) for use of their Cary 5000 Spectrophotometer. Portions of this work were supported by the Director, Office of Science (OS), Office of Basic Energy Sciences, of the U.S. Department of Energy (DOE) under Contract No. DE-AC02-05CH11231, and were carried out at SSRL, a Directorate of SLAC National Accelerator Laboratory and an OS User Facility operated for the DOE OS by Stanford University.

[1] a) *Electron Transfer in Inorganic, Organic, and Biological Systems, Vol. 228*, American Chemical Society, **1991**; b) L. E. Eberson, *Electron Transfer Reactions in Organic Chemistry; Reactivity and Structure, Vol. 25*, Springer, Heidelberg, **1987**; c) I. Bertini, H. B. Gray, S. J. Lippard, J. S. Valentine, *Biological Inorg. Chem.: Structure and Reactivity, Vol. 25*, University Science Books, Sausalito, CA, **2007**; d) G. H. B., J. R. Winkler, *Annu. Rev. Biochem.* **1996**, *65*, 537-561.

[2] a) A. J. Hoff, J. Deisenhofer, *Physics Reports* **1997**, *287*, 1-247; b) S. Ferguson-Miller, G. T. Babcock, *Chem. Rev.* **1996**, *96*, 2889-2908; c) S. Fukuzumi, *B. Chem. Soc. Jpn.* **1997**, *70*, 1-28; d) S. Fukuzumi, in *Inorg. Chem.Prog. Inorg. Chem.*, John Wiley & Sons, Inc., **2009**, pp. 49-154; e) S. Fukuzumi, *Electron Transfer in Chemistry*, Wiley-VCH, Weinheim, **2001**; f) S. Fukuzumi, *Organic & Biomolecular Chemistry* **2003**, *1*, 609-620; g) S. Fukuzumi, K. Ohkubo, *Coord. Chem. Rev.* **2010**, *254*, 372-385; h) S. Fukuzumi, Y. Morimoto, H. Kotani, P. Naumov, Y. M. Lee, W. Nam, *Nat. Chem.* **2010**, *2*, 756-759; i) K. Srinivasan, P. Michaud, J. K. Kochi, *J. Am.*

*Chem. Soc.* **1986**, *108*, 2309-2320; j) Y. J. Park, J. W. Ziller, A. S. Borovik, *J. Am. Chem. Soc.* **2011**, *133*, 9258-9261; k) D. C. Lacy, Y. J. Park, J. W. Ziller, J. Yano, A. S. Borovik, *J. Am. Chem. Soc.* **2012**, *134*, 17526-17535.

[3] a) S. Fukuzumi, K. Ohkubo, *Chemistry-a European Journal* **2000**, *6*, 4532-4535; b) K. Ohkubo, S. C. Menon, A. Orita, J. Otera, S. Fukuzumi, *Journal of Organic Chemistry* **2003**, *68*, 4720-4726.

[4] a) S. Cotton, *Lanthanide and Actinide Chemistry*, John Wiley & Sons Ltd, West Sussex, England, **2006**; b) H. C. Aspinall, *Chemistry of the f-block Elements, Vol. 1*, Overseas Publishing Company, UK, **2001**.

[5] a) J. R. Robinson, P. J. Carroll, P. J. Walsh, E. J. Schelter, *Angew. Chem., Int. Edit.* **2012**, *51*, 10159-10163; b) J. R. Robinson, P. J. Carroll, P. J. Walsh, E. J. Schelter, *Angew. Chem.* **2012**, *124*, 10306-10310.

[6] A. Sen, H. A. Stecher, A. L. Rheingold, *Inorg. Chem.* **1992**, *31*, 473-479.

[7] a) A. Kerridge, R. Coates, N. Kaltsoyannis, *J. Phys. Chem. A* **2009**, *113*, 2896-2905; b) A. Ashley, G. Balazs, A. Cowley, J. Green, C. H. Booth, D. O'Hare, *Chem. Commun.* **2007**, 1515-1517; c) A. Streitwieser, S. A. Kinsley, C. H. Jenson, J. T. Rigsbee, *Organometallics* **2004**, *23*, 5169-5175; d) M. D. Walter, C. H. Booth, W. W. Lukens, R. A. Andersen, *Organometallics* **2009**, *28*, 698-707; e) C. H. Booth, M. D. Walter, M. Daniel, W. W. Lukens, R. A. Andersen, *Phys. Rev. Lett.* **2005**, *95*, 267202.

[8] a) I. J. Casely, S. T. Liddle, A. J. Blake, C. Wilson, P. L. Arnold, *Chem. Commun.* **2007**, 5037-5039; b) M. D. Walter, R. Fandos, R. A. Andersen, *New J. Chem.* **2006**, *30*, 1065-1070; c) P. L. Arnold, I. J. Casely, S. Zlatogorsky, C. Wilson, *Helv. Chim. Acta* **2009**, *92*, 2291-2303.

[9] K. Okamoto, H. Imahori, S. Fukuzumi, *J. Am. Chem. Soc.* **2003**, *125*, 7014-7021.

[10] L. R. Morss, in *Standard Potentials in Aqueous Solution* (Eds.: A. J. Bard, R. Parsons, J. Jordan), Marcel Dekker, New York, **1985**, pp. 587-629.

[11] a) H. E. Hoefdraad, *J. Inorg. Nucl. Chem.* **1975**, *37*, 1917-1921; b) G. Brauer, H. Kristen, *Z. Anorg. Allg. Chem.* **1979**, *456*, 41-53; c) D. Han, T. Uda, Y. Nose, T. Okajima, H. Murata, I. Tanaka, K. Shinoda, *Adv. Mater.* **2012**, *24*, 2051-2053.

[12] D. E. Hobart, K. Samhoun, J. P. Young, V. E. Norvell, G. Mamantov, J. R. Peterson, *Inorg. Nucl. Chem. Lett.* **1980**, *16*, 321-328.

[13] a) A. J. Wooten, P. J. Carroll, P. J. Walsh, *J. Am. Chem. Soc.* **2008**, *130*, 7407-7419; b) A. J. Wooten, P. J. Carroll, P. J. Walsh, *Angew. Chem.-Int. Edit.* **2006**, *45*, 2549-2552.

[14] a) W. J. Evans, M. A. Hozbor, *J. Organomet. Chem.* **1987**, *326*, 299-306; b) R. Baggio, M. T. Garland, O. Pena, M. Perec, *Inorg. Chim. Acta* **2005**, *358*, 2332-2340; c) I. A. Setyawati, S. Liu, S. J. Rettig, C. Orvig, *Inorg. Chem.* **2000**, *39*, 496-507.

[15] a) T. Sakurai, *Acta Crystallogr.* **1965**, *19*, 320-&; b) T. Sakurai, *Acta Crystall. B-Stru.* **1968**, *B 24*, 403-&; c) J. Regeimbal, S. Gleiter, B. L. Trumpower, C. A. Yu, M. Diwakar, D. P. Ballou, J. C. A. Bardwell, *P. Natl. Acad. Sci. USA* **2003**, *100*, 13779-13784; d) R. Kuroda, Y. Imai, N. Tajima, *Chem. Commun.* **2002**, 2848-2849; e) R. Kuroda, T. Sato, Y. Imai, *Crystengcomm* **2008**, *10*, 1881-1890.

[16] a) G. A. Molander, C. R. Harris, *Chem. Rev.* **1996**, *96*, 307-338; b) H. B. Kagan, *Tetrahedron* **2003**, *59*, 10351-10372; c) A. Krief, A. M. Laval, *ChemiChem. Rev.* **1999**, *99*, 745-777; d) D. J. Procter, R. A. Flowers, *Organic Synthesis Using Samarium Diiodide: A Practical Guide*, Royal Society of Chemistry, Cambridge, England, **2010**.

[17] D. C. Bradley, J. S. Ghotra, F. A. Hart, *J. Chem. Soc. Dalton* **1973**, 1021-1027.

[18] R. K. Thomson, B. L. Scott, D. E. Morris, J. L. Kiplinger, *Cr. Chim.* **2010**, *13*, 790-802.

[19] G. M. Sheldrick, University of Gottingen, Germany, **2008**.

[20] Bruker, Bruker AXS Inc., Madison, Wisconsin, USA, **2009**.

[21] Bruker, Bruker AXS Inc., Madison, Wisconsin, USA, **2009**.

[22] G. M. Sheldrick, University of Gottingen, Germany, **2008**.

[23] G. M. Sheldrick, University of Gottingen, Germany, **2007**.

[24] G. M. Sheldrick, *Acta Crystallogr. A* **2008**, *64*, 112-122.

[25] P. Vandersluis, A. L. Spek, *Acta Crystallogr. A* **1990**, *46*, 194-201.

Received: ((will be filled in by the editorial staff))
Revised: ((will be filled in by the editorial staff))
Published online: ((will be filled in by the editorial staff))

**Entry for the Table of Contents** (Please choose one layout only)

Layout 1:

**Two on One!**

*Jerome R. Robinson, Corwin H. Booth, Patrick J. Carroll, Patrick J. Walsh* and Eric J. Schelter**

……...…… Page – Page

**Dimeric Rare Earth BINOLate Complexes: Activation of 1,4–Benzoquinone through Lewis-Acid Promoted Potential Shifts**

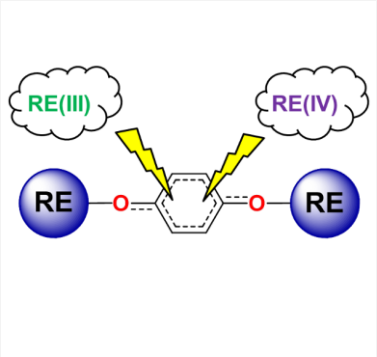


Reaction of *p*–benzoquinone (BQ) with a series of rare earth/alkali metal/1,1′–BINOLate (REMB) complexes (RE: La, Ce, Pr, Nd; M: Li) results in the largest recorded shift in reduction potential observed for BQ upon RE complexation. In the case of cerium, the formation of a 2:1 [Ce]:[BQ] complex shifts the two electron reduction of BQ by ≥ 1.6 V to a more favourable potential.

Layout 2:

**Catch Phrase** ——————————

*Author(s), Corresponding Author(s)** ……...… Page – Page

**Title Text**

((The TOC Graphic should not exceed the size of this area))

Text for Table of Contents, max. 450 characters.

Text for Table of Contents, continued.